Journal Pre-proof

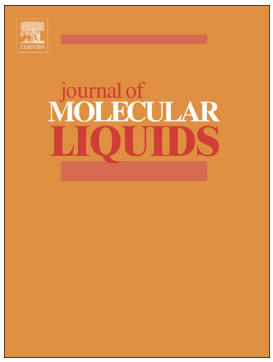

Influences of electric field strength on rheological properties of electrorheological fluid based on hollow poly (O-phenylenediamine co O-toluidine) dispersed on silicone oil

Cuong Manh Vu, Van-Huy Nguyen, Quang-Vu Bach

PII: S0167-7322(20)33695-3

DOI: https://doi.org/10.1016/j.molliq.2020.113762

Reference: MOLLIQ 113762

To appear in: *Journal of Molecular Liquids*

Received date: 7 June 2020

Revised date: 30 June 2020

Accepted date: 4 July 2020

Please cite this article as: C.M. Vu, V.-H. Nguyen and Q.-V. Bach, Influences of electric field strength on rheological properties of electrorheological fluid based on hollow poly (O-phenylenediamine co O-toluidine) dispersed on silicone oil, *Journal of Molecular Liquids* (2020), https://doi.org/10.1016/j.molliq.2020.113762

This is a PDF file of an article that has undergone enhancements after acceptance, such as the addition of a cover page and metadata, and formatting for readability, but it is not yet the definitive version of record. This version will undergo additional copyediting, typesetting and review before it is published in its final form, but we are providing this version to give early visibility of the article. Please note that, during the production process, errors may be discovered which could affect the content, and all legal disclaimers that apply to the journal pertain.

© 2020 Published by Elsevier.

Journal Pre-proof

Influences of Electric Field Strength on Rheological Properties of Electrorheological Fluid based on Hollow Poly (O-phenylenediamine co O-toluidine) Dispersed on Silicone Oil

Cuong Manh Vu[1,2], Van-Huy Nguyen[3,4*], Quang-Vu Bach[1]

[1]Center for Advanced Chemistry, Institute of Research and Development, Duy Tan University, Da Nang, Vietnam; vumanhcuong@duytan.edu.vn;

[2]Faculty of Chemical-Physical Engineering, Le Qui Don Technical University, 236 Hoang Quoc Viet, Bac Tu Liem, Ha Noi, Vietnam;vumanhcuong309@gmail.com

[3]Department for Management of Science and Technology Development, Ton Duc Thang University, Ho Chi Minh City, Viet Nam

[4]Faculty of Applied Sciences, Ton Duc Thang University, Ho Chi Minh City, Viet Nam

Corresponding author: Department for Management of Science and Technology Development, Ton Duc Thang University, Ho Chi Minh City, Viet Nam

V. H. Nguyen (nguyenvanhuy@tdtu.edu.vn)

Abstract

In this study, hollow poly (O-phenylenediamine-co-O-toluidine) (POPD-co-OT) was synthesized via oxidative polymerization reaction. The POPD-co-OT was decorated into polystyrene surface core spherical particles before removing the core to obtain the hollow particles. The chemical structure and morphology of the conducting POPD-co-OT were studied with FTIR spectroscopy, proton NMR, scanning electron microscopy, and TEM. The hollow particles were applied in the dispersion phase for the preparation of electrorheological fluid (ERF). The rheological properties were investigated with a rotational rheometer, whereas the chain formation inside the ERF was observed using OM. The experimental results indicated that the shear stress of ERF increased with increasing strength of the electric field and quickly responded by impacting the external electric field strength. The ERF system is quite stable for along time up to 200h.

Keywords: Hollow particles; poly (O-phenylenediamine-co-O-toluidine); electric field strength (E); chain formation; suspension; rheological characteristics.

1. Introduction

ERF is a type of smart material that the conducting or polarizable particles are well blended in an insulating liquid [1–4]. The rheological behaviors can be easily altered from liquid- to solid-like by adjusting the external field strength because of the formation of chains inside the rheological fluid [5]. This changing occurred in milliseconds [6] and is reversible by removing the external electric field strength. The distribution of conducting particles is random with no external field strength and the electrorheological fluids (ERFs) exhibit Newtonian fluid characteristics. By attaching the external field strength, the dispersed phases are polarized before forming chains or columns as a result of interactions between particles. The viscosity of the ERF varies instantaneously by changing the external electric field strength. Some rheological ERF characteristics including of shear stress, modulus and shear viscosity were improved by increasing the electric field strength [7]. This improvement helped expand ERF applications in industrial fields like hydraulics, electronics, and robotics [8–11].

Many dispersed materials such as core-shell structured particles, polymers, and inorganic particles have been successfully applied for the fabrication of ERF systems [12–16]. Conductive polymer-based materials have been also widely applied in the dispersion phase because of their advantages such as low electrical conductivity and a π-conjugated structure [17–19]. Polyaniline (PANI) and its derivatives were considered promising conducting polymers for ERF applications because of their low cost, easy preparation, excellent environment stability, and electric conductivity control [20–24]. Many types of PANI and its derivatives based on composite materials have been applied in the dispersion phase for ERF. The core/shell particles based on PANI were prepared and examined in detail with excellent response [25–27]. The high density of these phases was considered the primary

disadvantage which induced ERF dispersion stability. This problem has been resolved with the use of many hollow low-density particles to replace the high-density core-shell particles [28–30].

In the present work, hollow poly (p-toluidine-co-p-phenylenediamine) was synthesized via simple method before being used in the dispersion phase in the ERF system. The poly (p-toluidine-co-p-phenylenediamine) shell was decorated onto the surface of a polystyrene core, which was previously synthesized via surfactant free emulsion polymerization. The PS particles were modified with sulfonic acid to form sulfonated PS spherical particles prior to coating with a conducting polymer shell. The toluidinium and phenylenediaminium ions were formed in an acidic medium and easily interacted with the sulfonate ion because of the well-coated layer of poly (p-toluidine-co-p-phenylenediamine) on the core of the PS spherical particles. The PS core was removed by proper solvent before obtaining the hollow conductive poly (POPD-co-OT). The ERF was fabricated by dispersion of a hollow conductive poly (POPD-co-OT) in a silicone oil medium with a high speed mechanical stirrer and ultrasonication technique. Many characteristics of the ERF system were investigated.

2. Experimental

2.1. Materials

P-toluidine, p-phenylenediamine, silicone oil, HCl (37%), styrene monomer, H_2SO_4, and potassium persulfate (PPS) (≥99%) were supplied by Sigma-Aldrich (Vietnam).

2.2. Fabrication of hollow POPD-co-OT

Three synthesization steps were applied to receive the hollow poly (p-toluidine-co-p-phenylenediamine):

Step 1: The PS spherical particles were prepared via surfactant-free emulsion polymerization reaction.

Approximately 25 g of styrene was stirred with 300 g of distilled water in one necked glass flask. The temperature was raised from room temperature to 75 °C before adding of 0.5 g of ammonium

persulfate (APS). The reaction was kept at 75 °C for one day at 200 rpm. The PS sphere was obtained by washing the product with distilled water 4 times with a centrifuge and drying in lab oven at 65 °C for 24h before receiving the powder product.

Step 2: Fabrication of the PS@ poly (POPD-Co-OT) core/shell particles

Approximately 0.5 g of PS particles was stirred in 40 mL of sulfuric acid (98 %) in a one-necked glass flask at 45 °C for 6.5 h at 200 rpm. The sulfonate was collected after washing several times with distilled water. The sulfonated PS spheres were then dispersed in distilled water before adding P-toluidine (0.1 g), P-phenylenediamine monomer (0.1 g), and 5 mL of HCl 1M solution. Next, 0.1 g of APS was mixed with above mixture, and maintained at 0 °C for one day. The products were washed several times with distilled water before drying in a lab oven at 65 °C for another one day.

Step 3: Removal of the PS core to obtain the hollow poly (POPD-co-OT)

The core-shell PS@ poly (POPD-co-OT) particles were stirred with toluene solvent for one day at ambient condition to remove the cores. The hollow poly (POPD-co-OT) particles were received from washing and processed with distilled water before drying in lab oven at 65 °C for 24 h. The processing details are presented in Figure 1:

Figure 1

Figure 2

2.3. ERF preparation

The hollow POPD-co-OT particles were well blended with silicone oil (weight fraction of 60 wt.%) by simultaneous using of a homogenizator at 100 rpm for 2 h and a sonication technique for another 1 h.

2.4. Characterization methods

The morphology and inside structure were observed by using of a scanning electron microscopy (SEM), and a transmission electron microscopy (TEM). The densities were determined with help of

a AccuPyc 1340 gas pycnometer (USA). The conductivity was determined with help of a MCP-T610 resistivity meter (Japan).

The chemical structure was examined using Fourier Transform Infrared Spectroscopy and proton nuclear magnetic resonance (^{1}H-NMR). The dynamic light scattering method was used via an equipment of Malvern Zetasizer ZS90 (England).

The chain formation was confirmed with help of a Optical microscopy (OM). The rheological characteristics were studied with a rotational rheometer that was conected with a high voltage generator. The dielectric behaviors were investigated with an LCR meter (HP 4284A Precision) with the frequency ranging from 20 Hz to 1 MHz at room temperature.

The stability of ERF system was characterized by the sedimentation percent. The ERF was poured into a tube and the height of particle subsided was oserved for about 200h. The sedimentation percent was caculated by following equation:

$$\text{Sedimentation percent} = \frac{H_p}{H_0} X 100 \ (\%)$$

H_p (cm), H_0 (cm) are the height of particle subsided, and the total height of suspension in tube, respectively [31].

3. Results and discussion

Figure 3

The SEM images of the PS sphere and the PS@ poly (POPD-Co-OT) and hollow poly (POPD-Co-OT) particles are shown in Figure 3. The PS sphere exhibited a smooth surface, spherical shape, and size of approximately 450 nm. The PS@ poly (POPD-Co-OT) and hollow poly (POPD-Co-OT) showed rougher surfaces with sizes of approximately 550 nm. The diameter of the hollow particles (approximately 100 nm) was larger than that of spherical PS particles. This value corresponds to the thickness of both the core-shell and hollow particles. The densities of the PS sphere, the PS@ poly (POPD-Co-OT), and the hollow poly (POPD-Co-OT) were 1.18, 1.38, and 0.96 g/cm^3, respectively. The hollow poly (POPD-Co-OT) expressed conductivity of approximately 5.1×10^{-11} S.cm^{-1}.

The SEM technique was applied to observe the surface morphology (Figure 3).

Figure 3

The PS particles showed a smooth surface and a diameter of approximately 460 nm. The PS@ poly (POPD-Co-OT) and hollow poly (POPD-Co-OT) particles exhibited rougher surfaces and diameters of approximately 500 nm. The SEM image of hollow poly (POPD-Co-OT) particles after sonicating was also presented in Figure 3 D. The Figure 3D indicated that the hollow particles were not broken by sonication processing. The inner structure morphologies of the PS sphere, the PS@ poly (POPD-Co-OT), and the hollow poly (POPD-Co-OT) were studied with a TEM technique (Figure 4).

Figure 4

The PS particles showed their fully solid structure with black images (Figure 4a). Figure 4b shows the black core and gray shell in the morphology of the PS@ poly (POPD-Co-OT) particles. After removing the black core, the hollow structure only has a gray shell (Figure 4c). The thickness of the hollow particles was about 40 nm. Fig. 4c indicates the good chemical resistance of the high-strength poly (POPD-Co-OT) shell because the poly (POPD-Co-OT) maintained its spherical form after the etching process.

The chemical structures of PS, PS@ poly (POPD-Co-OT), and hollow poly (POPD-Co-OT) particles were examined with an FTIR technique (Figure 5).

Figure 5

The PS particles showed peaks at 3028 cm^{-1}, which assigned for the C-H of the aromatic ring. The signal at 2922 and 2852 cm^{-1} was assigned to the C-H in the main chain. Additionally, the signals of C-C stretching, aromatic vibration, CH_2 bending, C-H out-of-plane bending, and C-C out of plane bending in the benzene ring occurred at peaks of 1601, 1493, 1452, 755, and 698 cm^{-1}. The signals in the range of 1700–2000 cm^{-1} were assigned to the benzene ring overtones [32, 33].

The FTIR spectra of PS@ poly (POPD-Co-OT) revealed several new peaks when compared to the FTIR spectra of pure PS particles (Figure 4b). The signal at 3390 cm^{-1} was assigned to the N-H. The

stretching vibration of C=N, C=C of quinonoid and benzenoid rings occurred at 1596 and 1505 cm^{-1}, respectively [34–36]. The peak of the C-N stretching of the benzenoid ring occurred at a wavenumber of 1246 cm^{-1}. The phenazine structure occurred at the peak of 850 cm^{-1}. The FTIR spectra of PS@ poly (POPD-Co-OT) and hollow poly (POPD-Co-OT) are identical because of the characteristics of the FTIR technique, which only affects the surface instead of the inner depths of the core-shell particle.

The hollow particle proton NMR is presented in Figure 6.

Figure 6

The aromatic ring, amine group (NH_2), and CH_3 protons occurred at the chemical shifts of 6.6, 3.65, and 3.4 ppm, respectively.

The above results helped confirm the success of the fabrication of hollow poly (POPD-Co-OT).

The dynamic light scattering method was applied to determine the diameter of the PS sphere and the hollow poly (POPD-Co-OT) (Figure 7).

Figure 7

The average diameter of the PS sphere and the hollow poly (POPD-Co-OT) particles were 460 and 502 nm, respectively. Thus, the thickness of the hollow particle by this method was approximately 42 nm.

Hollow poly (POPD-Co-OT) was the principal material used in the fabrication of the ERF system by dispersion in silicone oil with 60 wt. %. The ERF behavior under the application of external electric fields was fully examined. The chain formation, which was considered as one of the most important ERF characteristics, was obtained by OM (Figure 8).

Figure 8

The hollow POPD-co-OT) was randomly distributed without of external electric field (Figure 8a). By applying an electric field, the chain of particles was swiftly formed (Figure 8b) [37].

Figure 9 presents the rheological characteristics of ERF.

Journal Pre-proof

Figure 9

With no electric field, the ERF exhibited almost Newtonian characteristics with a linear relationship between the shear stress and the shear rate (Figure 9a). Additionally, the shear viscosity was constant from moderate share rate values (Figure 9b). When electric field strength was applied, the ERF showed non-Newtonian characteristic with the appearance of plateau regions of shear stress in regions of low share rate values because of the chain formation phenomenon. The share stress was then increased in regions with a higher share rate. Moreover, the shear viscosity decreased with increasing shear rate as result of the breaking of chain structures in the ERF system by shear flow. This characteristic was assigned to shear thinning characteristic. With enlarging of electric field strength, the share rate and shear viscosity increased and did not conform to the Bingham model [38]. The Choi-Choi-Jhon (CCJ) model was applied to describe this suspension as follows:

$$\tau = \frac{\tau_0}{(1+(t_1\,\dot{y})^{\alpha}} + \eta_{\infty}\left(1+\frac{1}{(t_2\,\dot{y})^{\beta}}\right)\dot{y} \quad (1)$$

The CCJ model was characterized by several parameters (as seen in Table 1), τ_0, t_i (t_1, t_2), η_{∞}, α, β, which corresponded to dynamic shear stress, constant times, shear viscosity at the limitless shear rate ($\dot{y}$) region, descent range of shear stress in the low $\dot{y}$ area, exponent at high shear rate areas, and ($(0 < \beta \leq 1$, because of $\frac{d\tau}{dy} \geq 0)$, respectively.

Table 1

The transformation inside the ERF by applying the external E was characterized by a factor called ERF efficiency, which was calculated from the following equation:

$$e = \frac{(\eta_E - \eta_0)}{\eta_0}, (2)$$

Journal Pre-proof

In this equation, η_E and η_0 were the viscosity of ERF with presence and absence an E, respectively. The ERF efficiency and shear rate diagrams are showed in Fig. 9c with improving of ERF efficiency by enlarging of E.

Figure 10

The viscous and elastic behaviors of the ERF system were received via oscillation test. The angular frequency was set to 6.26 rad.s^{-1} before finding the linear viscoelastic region. The strain varied from 10^{-3} to 1 (%). Two valuable factors (storage modulus (G') and loss modulus (G'')) were received from this test. The storage modulus was generally characterized by elastic behavior, which symbolized the deformation energy reserve in the material. The G'' corresponded with elastic property and was depicted by the consumed deformation energy in the material. In the low-strain (plateau) region, the value of G' was always higher than that of G''. In this region, the chains of the dispersed phase were formed and considered as the primary cause of the supercilious elastic property when compared to the viscous property. When the strain value was greater than the value of the plateau region, both G' and G'' exhibited a decreasing trend. The value of G'' in this region outdistanced that of G'. This signifies that the viscous property prevailed over the elastic property as a result of the broken chain-like structure.

A graph of elastic stress ($\tau' = G'.\gamma$) versus strain was plotted to find the transition point in the broken chain-like structure in the ERF system with shear flow (Figure 10b). Figure 10b indicates that at a low strain value ($\gamma < 0.1$), the elastic stress linearly increased as strain increased. The chain-like structure was broken at strain values higher than 0.1. The elastic yields stress was determined at the peak of stress-strain curve. Figure 10b also indicates that the elastic stress improved with increasing E.

Figure 11 presents the plots of yield stress τ_y and E.

Figure 11

Two yield stress values—dynamic and elastic—were determined for each E value. The elastic yield stress (EYS) was received from the dynamic oscillation tests (Figure 10b). The dynamic yield stress (DYS) was acquired from the controlled shear rate (CSR) tests using the CCJ model (Figure 9a). The mutual connection between yield stress, τ_y, and E was depicted via following equation:

$$\tau_y \alpha E^{\alpha} \quad (3)$$

The value of α was used as an indicator for the determination of a conduction (α=1.5) or polarization (α=2) model of the ERF system. The DYS was higher than that of the EYS (Figure 11). Both EYS and DYS were fitted to the polarization model with an α value of approximately 2.

The responsiveness of the ERF system with on-off procedure was also measured (Figure 12).

Figure 12

In this experiment, the shear rate was maintained at a constant value (γ = 1.5 s^{-1}), and the time between on and off was 50 s. The results in Fig. 12 indicate that the shear stress promptly increased to a specific value when an E was applied before decreasing to 0. The changing from a solid- to liquid-like structure was swift and reversible.

LCR testing was continuously used to obtain the dielectric properties of the ERF system in relation to the dielectric constant (ε') and dielectric loss (ε'') versus frequency (Figure 13).

Figure 13

A Cole-Cole plot was built based on the following equation [39]:

$$\varepsilon^* = \varepsilon' - i\varepsilon'' = \varepsilon_\infty + \frac{\varepsilon_0 - \varepsilon_\infty}{1 + (i\omega\lambda)^{(1-\alpha)}}, 0 \le \alpha \le 1, \quad (4)$$

Where, ε_0 and ε_∞ (as listed in Table 2) are the dielectric constant at zero and infinite frequencies, respectively. The difference of ε_0, and ε_∞ ($\varepsilon_0 - \varepsilon_\infty$) characterized the polarizability of the ERF system. λ is the relaxation time. The speed of polarization was mirrored with a λ value of $0.5\Pi f_{max}$; f_{max} is the maximum dielectric loss value. The difference (1-α) was the distribution of λ in the complete frequency range.

Table 2

The values of ε_0 and ε_∞ were 2.56 and 1.8, respectively, indirectly suggesting that the dispersed phases promptly responded to electric field strength. The value of relaxation time was 0.00026 s^{-1}, meaning that the hollow poly (POPD-Co-OT) particles were quickly polarized.

The plot of sedimentation percent versus time was shown in Figure 14.

Figure 14

The results in Figure 14 indicated that after 175h the ERF system tended to set steady state with sedimentaion percent was about 91.3 %. These results mean that the poly (POPD-Co-OT) based ERF system can keep stable for along time as a result of low density of hollow poly (POPD-Co-OT) particles.

4. Conclusions

In the present study, we prepared hollow poly (POPD-Co-OT) via co-oxidative polymerization reaction using polystyrene as a template. The chemical structure of poly (POPD-Co-OT) was confirmed with FTIR and ^{1}H-NMR techniques. The surface morphology, bulk structure, and diameter of the hollow particle were examined using SEM, TEM, and dynamic light scattering. The hollow poly (POPD-Co-OT) based ER fluid was fabricated, and its non-Newtonian behavior with the application of an external EFS was confirmed. The CCJ model was applied to fit the experimental data of the flow curves. The ERF system was fitted to the polarization model; the relationship between the yield stress τ_y and E was $\tau_y \alpha E^2$. Moreover, the G', G'' exhibited increasing trends as the electric field strength increased. The G' was higher than G'' at the low strain region as a result of fibrillation behavior with dominant elastic properties. The transition point corresponding to the broken solid-like structure was determined via the relation of elastic stress and strain. LCR testing indicated that the dispersion phase can be quickly polarized by applying an external E. Furthermore, a quite good dispersion stability was examined by a sedimentation percent.

Journal Pre-proof

Funding: This research was funded by the Vietnam National Foundation for Science and Technology Development (NAFOSTED) under grant number 104.02-2017.15.

References

1. X. Guo, Y. Chen, M. Su, D. Li, G. Li, C. Li, Y. Tian, C. Hao, Q. Lei, Enhanced Electrorheological Performance of Nb-Doped TiO2 Microspheres Based Suspensions and Their Behavior Characteristics in Low-Frequency Dielectric Spectroscopy, ACS. Appl. Mater. Interfaces. 7 (2015) 26624-26632.
2. S. Lee, J. Lee, S.H. Hwang, J. Yun, J. Jang, Enhanced Electroresponsive Performance of Double-Shell SiO2/TiO2 Hollow Nanoparticles, ACS. Nano. 9 (2015) 4939-4949.
3. J.A. Marins, B.G. Soares, Ionic liquid-based organically modified silica for the development of new electrorheological fluids. Colloid. Surface A. 529 (2017) 311-319.
4. C. Wang, L. Ma, Q. Wen, B. Wang, R. Han, C. Hao, K. Chen, Enhanced electrorheological characteristics of titanium oxide@$H_2Ti_2O_5$ nanotube core/shell nanocomposite, Colloid. Surface A. 578 (2019) 123641.
5. J.B. Yin, X.P. Zhao, Electrorheological fluids based on glycerol-activated titania gel particles and silicone oil with high yield strength, J. Colloid. Interf. Sci. 257 (2003) 228-236.
6. J. Noh, C.M. Yoon, J. Jang, Enhanced electrorheological activity of polyaniline coated mesoporous silica with high aspect ratio, J. Colloid. Interf. Sci. 470 (2016) 237-244.
7. A.V. Egorysheva, A.S. Kraev, O.M. Gajtko, T.V. Kusova, A.E. Baranchikov, A.V. Agafonov, V.K. Ivanov, High electrorheological effect in $Bi_{1.8}Fe_{1.2}SbO_7$ suspensions, Powder. Technol. 360 (2020) 96-103.
8. K.X. Wei, Q. Bai, G. Meng, L. Ye, Vibration characteristics of electrorheological elastomer sandwich beams, Smart Mater. Struct. 20 (2011) 055012.

9. M.A. Rkabi, H. Moeenfard, J. Rezaeepazhand, Vibration attenuation of rotor-bearing systems using smart electro-rheological elastomer supports, J. Braz. Soc. Mech. Sci. Eng. 41 (2019) 258.

10. J.H. Wu, G.J. Xu, Y.C. Cheng, F.H. Liu, J.J. Guo, P. Cui, The influence of high dielectric constant core on the activity of core–shell structure electrorheological fluid, J. Colloid. Interf Sci. 378 (2012) 36-43.

11. X. Tian, K. He, C. Wang, Q. Wen, B. Wang, S. Yu, C. Hao, K. Chen, Q. Lei, Preparation and electrorheological behavior of anisotropic titanium oxide/polyaniline core/shell nanocomposite, Compos. Sci. Tech. 137 (2016) 118-129.

12. S. Goswami, P. Gonçalves, M.T. Cidade, Electrorheological behavior of suspensions of camphorsulfonic acid (CSA) doped polyaniline nanofibers in silicone oil, Phys. Scr. 92 (2017) 075801.

13. X. Tian, K. He, B. Wang, S. Yu, C. Hao, K. Chen, Q. Lei, Flower-like Fe_2O_3/polyaniline core/shell nanocomposite and its electroheological properties, Colloid. Surfaces A. 498 (2016) 185-193.

14. X. Liu, H. Song, W. Sun, B. Wang, P. Zhang, X. Yuan, Z. Wang, X. Li, Strong nano size effect of titanium silicalite (TS-1) zeolites for electrorheological fluid, Chem. Eng. J. 384 (2020) 123267.

15. M.J. Espin, A.V. Delgado, L. Rejon, Electrorheologial properties of hematite/silicone oil suspensions under DC fields, J. Non-Newton. Fluid. 125 (2005) 1-10.

16. E. Kutalkova, T. Plachy, M. Sedlacik, On the enhanced sedimentation stability and electrorheological performance of intelligent fluids based on sepiolite particles, J. Mol. Liq. 309 (2020) 113120.

Journal Pre-proof

17. Q. Cheng, V. Pavlinek, Y. He, Y. Yan, C. Li, P. Saha, Template-free synthesis of hollow poly(o-anisidine) microspheres and their electrorheological characteristics, Smart. Mater. Struct. 20 (2011) 065014.

18. H. Yilmaz, H.I. Unal, B. Sari, Synthesis, characterization and electrorheological properties of poly(otoluidine)/Zn conducting composites, J. Appl. Polym. Sci. 103 (2007) 1058–1065.

19. Q. Cheng, V. Pavlinek, A. Lengalova, C. Li, Y. He, P. Saha, Conducting polypyrrole confined in ordered mesoporous silica SBA-15 channels: preparation and its electrorheology Micropor, Mesopor. Mater. 93 (2006) 263–269.

20. J.A. Marins, F. Giulieri, B.G. Soares, G. Bossis, Hybrid polyaniline-coated sepiolite nanofibers for electrorheological fluid applications, Synth. Met. 185 (2013) 9–16.

21. J. Tang, X. Wen, Z. Liu, J. Wang, P. Zhang, Synthesis and electrorheological performances of 2D PANI/TiO2 nanosheets, Colloid. Surfaces A. 552 (2018) 24-31.

22. J. Yin, X. Zhao, X. Xia, L. Xiang, Y. Qiao, Electrorheological fluids based on nano-fibrous polyaniline, Polymer. 49 (2008) 4413-4419.

23. J. Y. Hong, E. Kwon, J. Jang, Fabrication of silica/polythiophene core/shell nanospheres and their electrorheological fluid application, Soft. Matter. 5 (2009) 951.

24. T. Plachy, M. Sedlacik, V. Pavlinek, J. Stejskal, The observation of a conductivity threshold on the electrorheological effect of p-phenylenediamine oxidized with p-benzoquinone, J. Mater. Chem. C, 2015, 3, 9973-9980

25. Q. Wen, L. Ma, C. Wang, B. Wang, R. Han, C. Hao, K. Chen, Preparation of core–shell structured metal–organic framework@PANI nanocomposite and its electrorheological properties, RSC. Adv. 9 (2019) 14520-14530.

26. J. Yin, X. Wang, R. Chang, X. Zhao, Polyaniline decorated graphene sheet suspension with enhanced electrorheology, Soft. Matter 8 (2012) 294–297.

27. J. Yin, X. Xia, X. Wang, X. Zhao, The electrorheological effect and dielectric properties of suspensions containing polyaniline@titania nanocable-like particles, Soft. Matter. 7 (2011) 10978–10986.

28. B.H. Sung, U.S. Choi, H.G. Jang, Y.S. Park, Novel approach to enhance the dispersion stability of ER fluids based on hollow polyaniline sphere particle, Colloid. Surface A. 274 (2006) 37-42.

29. Q.L. Cheng, V. Pavlinek, Y. He, Y. Yan, C. Li, P. Saha, Synthesis and electrorheological characteristics of sea urchin-like TiO_2 hollow spheres, Colloid. Polym. Sci. 289 (2011) 799-805.

30. M. Sedlacik, M. Mrlik, V. Pavlinek, P. Saha, O. Quadrat, Electrorheological properties of suspensions of hollow globular titanium oxide/polypyrrole particles, Colloid. Polym. Sci. 290 (2012) 41-48.

31. M. Sedlačík, M. Mrlík, V. Pavlínek, P. Sáha, O. Quadrat, Electrorheological properties of suspensions of hollow globular titanium oxide/polypyrrole particles, Colloid. Polym. Sci. 290 (2012) 41–48

32. H.-D. Wu, S.-C. Wu, I.-D. Wu, F.-C. Chang, Novel determination of the crystallinity of syndiotactic polystyrene using FTIR spectrum, Polymer. 42 (2001) 4719-4725.

33. S. Das, H. Mahalingam, Exploring the synergistic interactions of TiO_2, rGO, and g-C_3N_4 catalyst admixtures in a polystyrene nanocomposite photocatalytic film for wastewater treatment: Unary, binary and ternary systems, J. Environmen. Chem. Eng. 7 (2019) 103246.

34. V.S. Sumi, S.R. Arunima, M.J. Deepa, M. Ameen Sha, A.H. Riyas, M.S. Meera, Viswanathan, S. Saji, S.M.A. Shibli, PANI-Fe_2O_3 composite for enhancement of active life of alkyd resin coating for corrosion protection of steel, Mater. Chem. Phys. 247 (2020) 122881.

35. A. Roy, A. Ray, P. Sadhukhan, K. Naskar, G. Lal, R. Bhar, C. Sinha, S. Das, Polyaniline-multiwalled carbon nanotube (PANI-MWCNT): Room temperature resistive carbon monoxide (CO) sensor, Synthet. Metals. 245 (2018) 182-189.

36. H. Wang, P. Shi, M. Rui, A. Zhu, R. Liu, C. Zhang, The green synthesis rGO/Fe_3O_4/PANI nanocomposites for enhanced electromagnetic waves absorption, Prog. Org. Coat. 139 (2020) 105476.

37. Q.-V. Bach, C.M. Vu, H.T. Vu, D.D. Nguyen, Suspension of poly(o-toluidine)-coated silica-based core–shell-structured composite in silicone oil: fabrication and rheological properties at different external electric field strengths, Polym. Bull. 77 (2020) 3563–3576.

38. Y. Meheust, K.P.S. Parmar, B. Schjelderupsen, J.O. Fossum, The electrorheology of suspensions of Na-fluorohectorite clay in silicone oil, J. Rheol. 55 (2011) 809.

39. C. M. Vu, Q.-V. Bach, H.T. Vu, V.-H. Nguyen, D.D. Nguyen, S.W. Chang, Influence of electric field strength on the rheological behavior of electro-rheological fluid based on poly(o-toluidine)-coated silica, J. Mol. Liq. 301 (2020) 112462.

Figures and Tables:

Figure 1: Fabrication processing of hollow poly (POPD-Co-OT)

Figure 2: The co-oxidative polymerization mechanism of poly (POPD-Co-OT)

Figure 3: Surface morphology of polystyrene (A), poly (POPD-Co-OT)/polystyrene core-shell particle (B), and hollow poly (POPD-Co-OT) (C)

Figure 4: The TEM images of polystyrene (A), poly (POPD-Co-OT)/polystyrene core-shell particle (B), and hollow poly (POPD-Co-OT) (C)

Figure 5: FTIR spectra of polystyrene (A), poly (POPD-Co-OT)/polystyrene core-shell particle (B), and hollow poly (POPD-Co-OT) (C)

Figure 6: ^{1}H-NMR of hollow poly (POPD-Co-OT)

Figure 1:

Journal Pre-proof

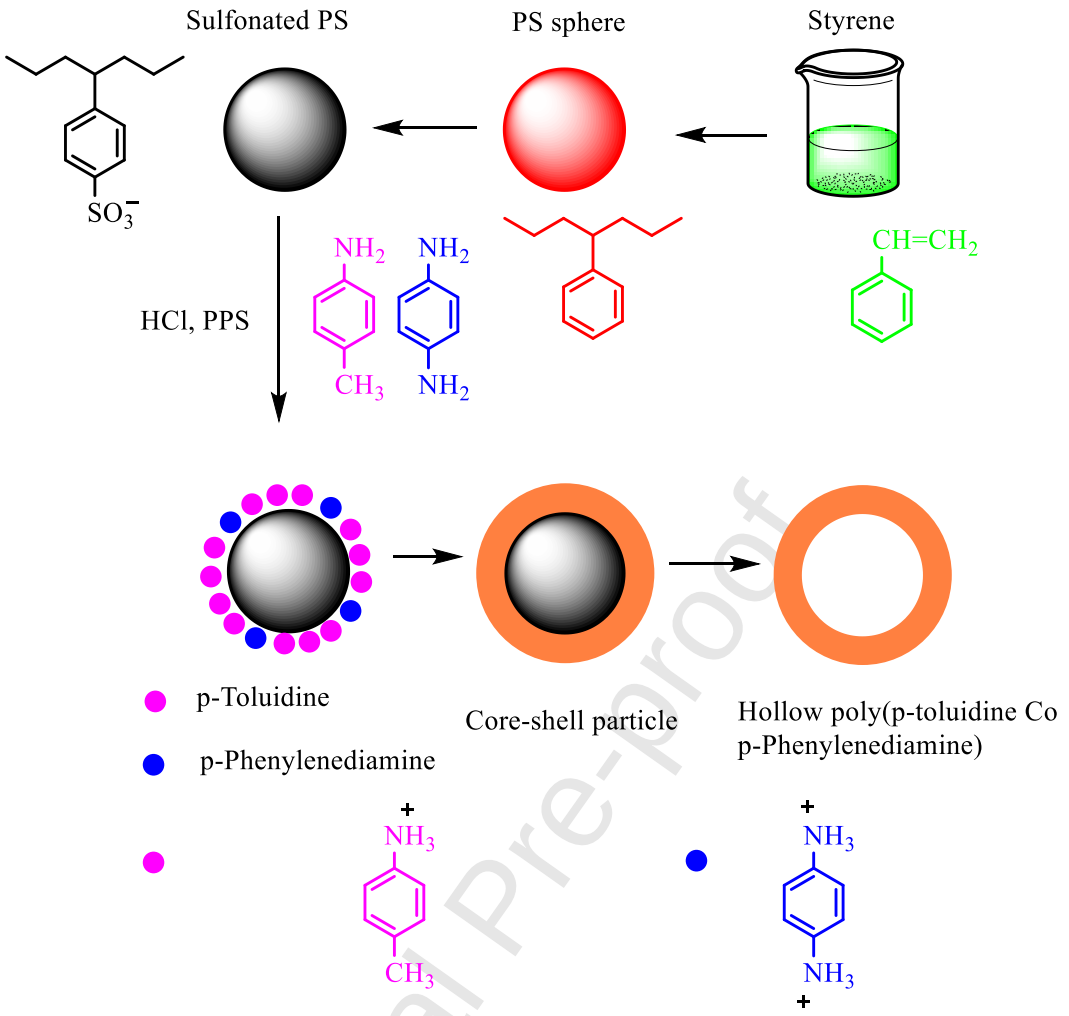

Figure 2:

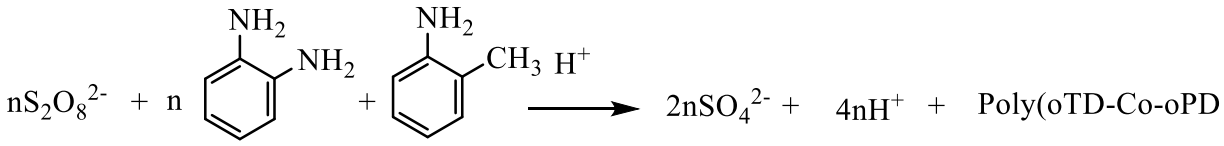

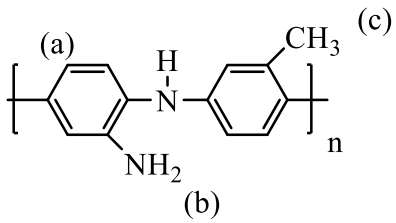

Journal Pre-proof

Figure 3:

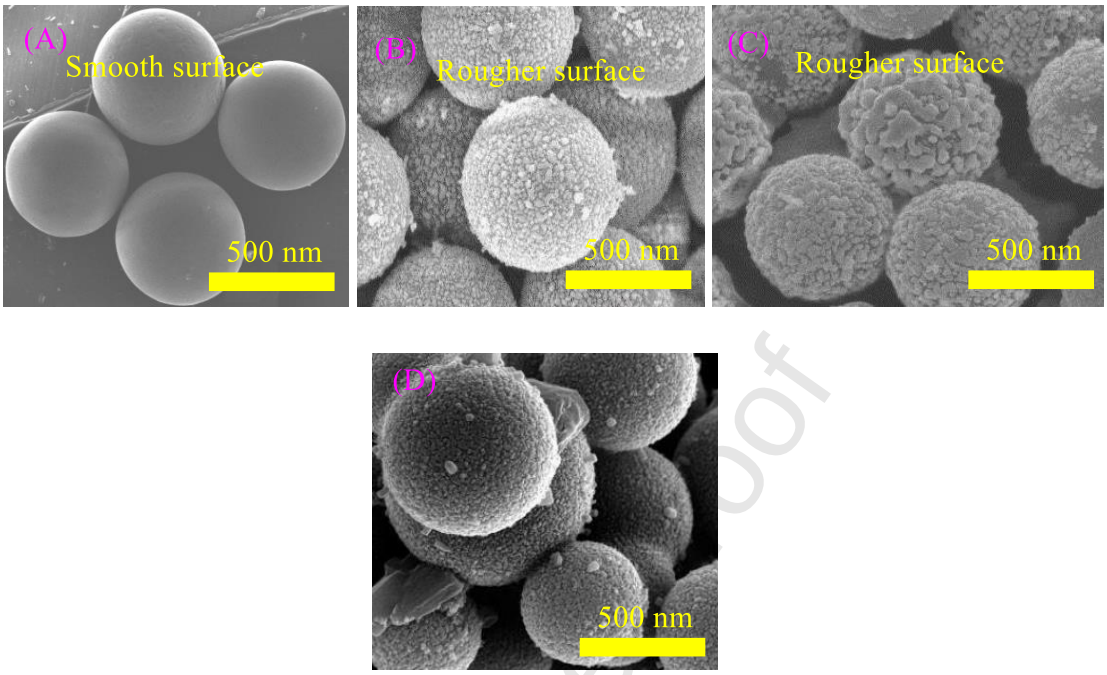

Figure 4:

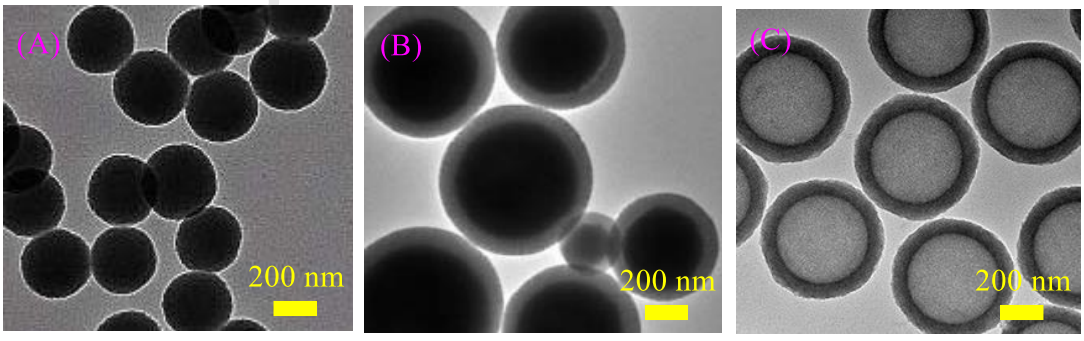

Figure 5:

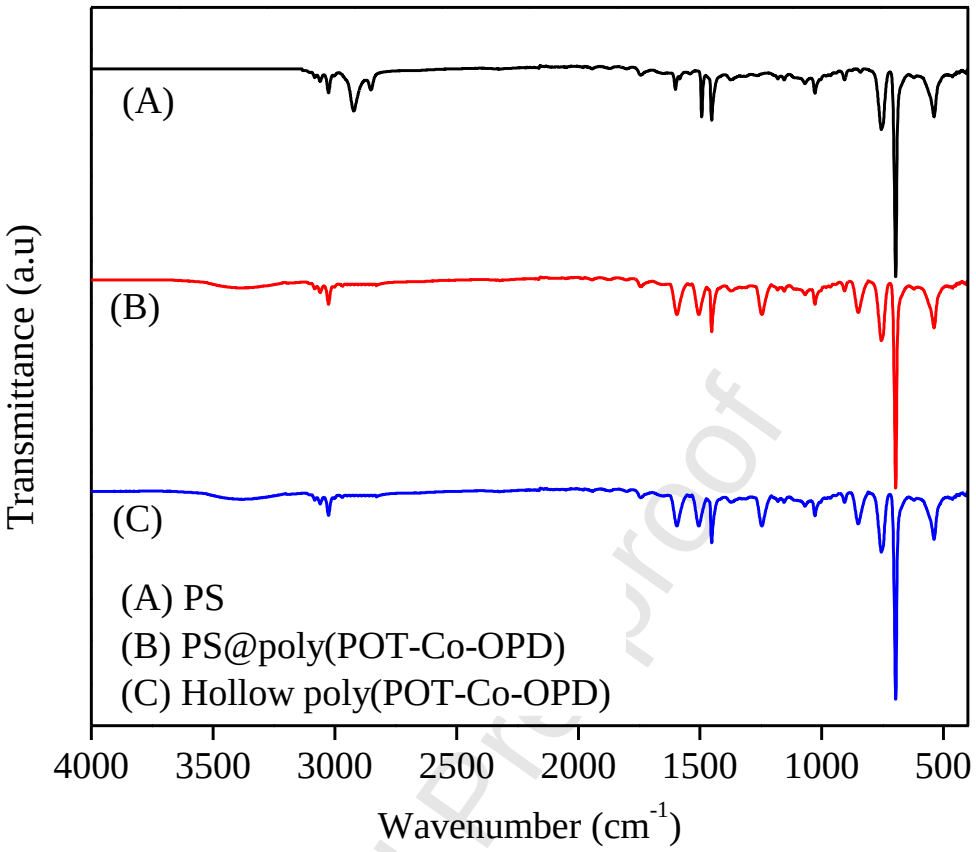

Journal Pre-proof

Figure 6:

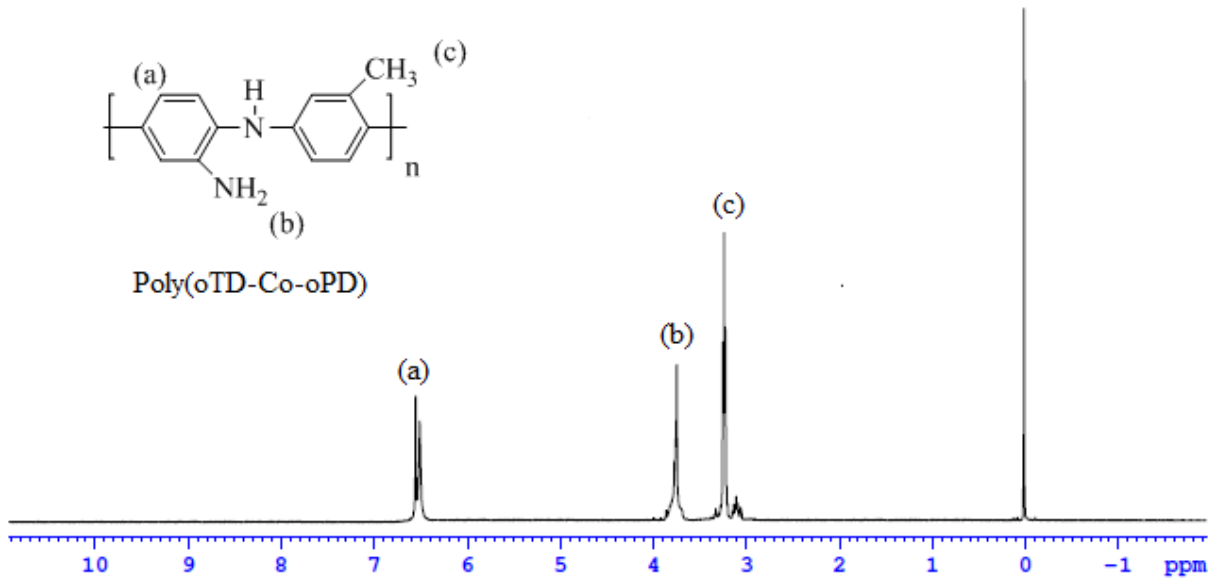

Figure 7:

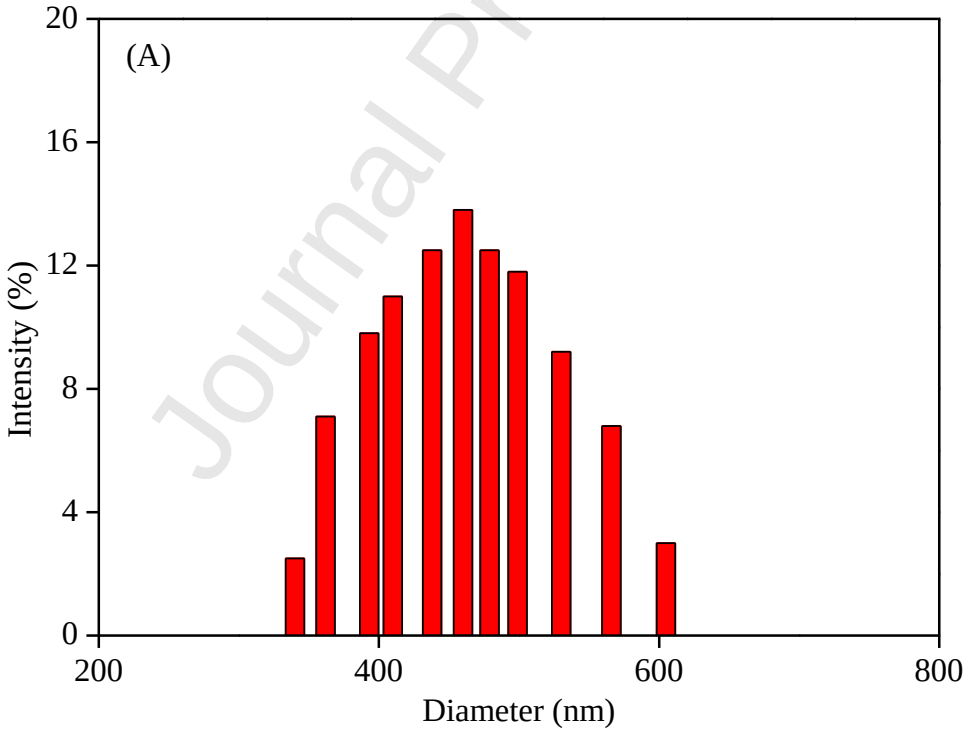

Journal Pre-proof

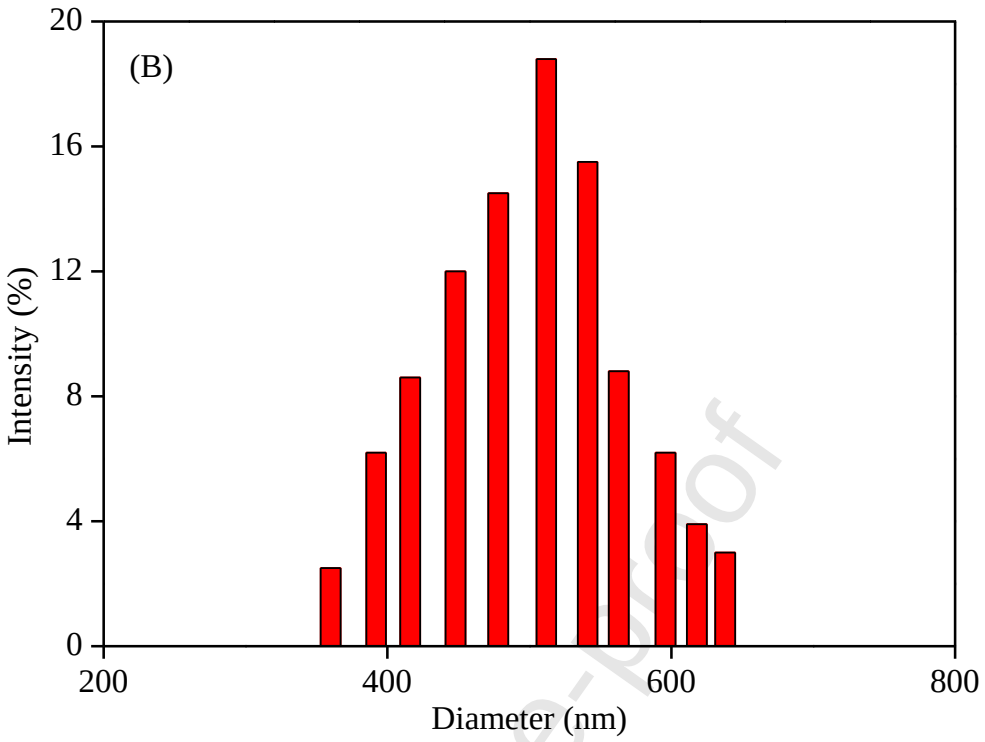

Figure 8:

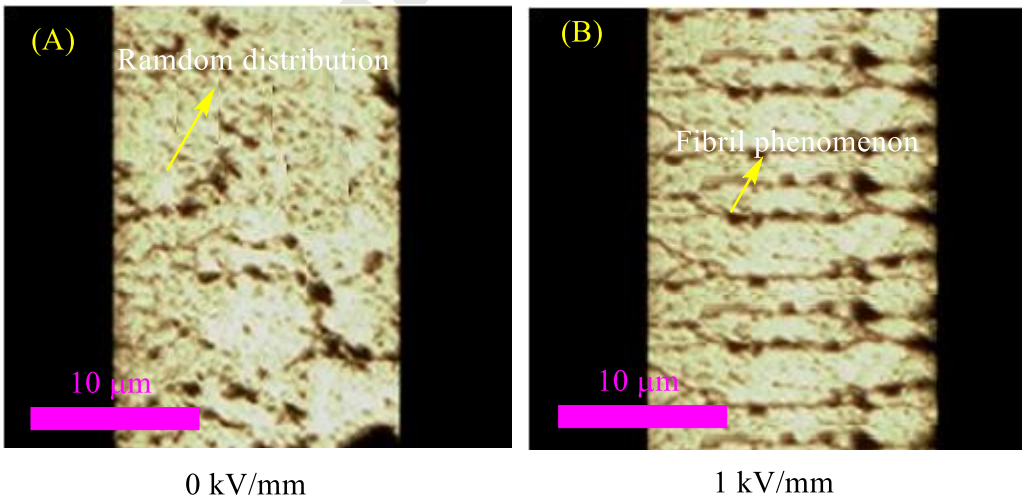

0 kV/mm 1 kV/mm

Journal Pre-proof

Figure 9:

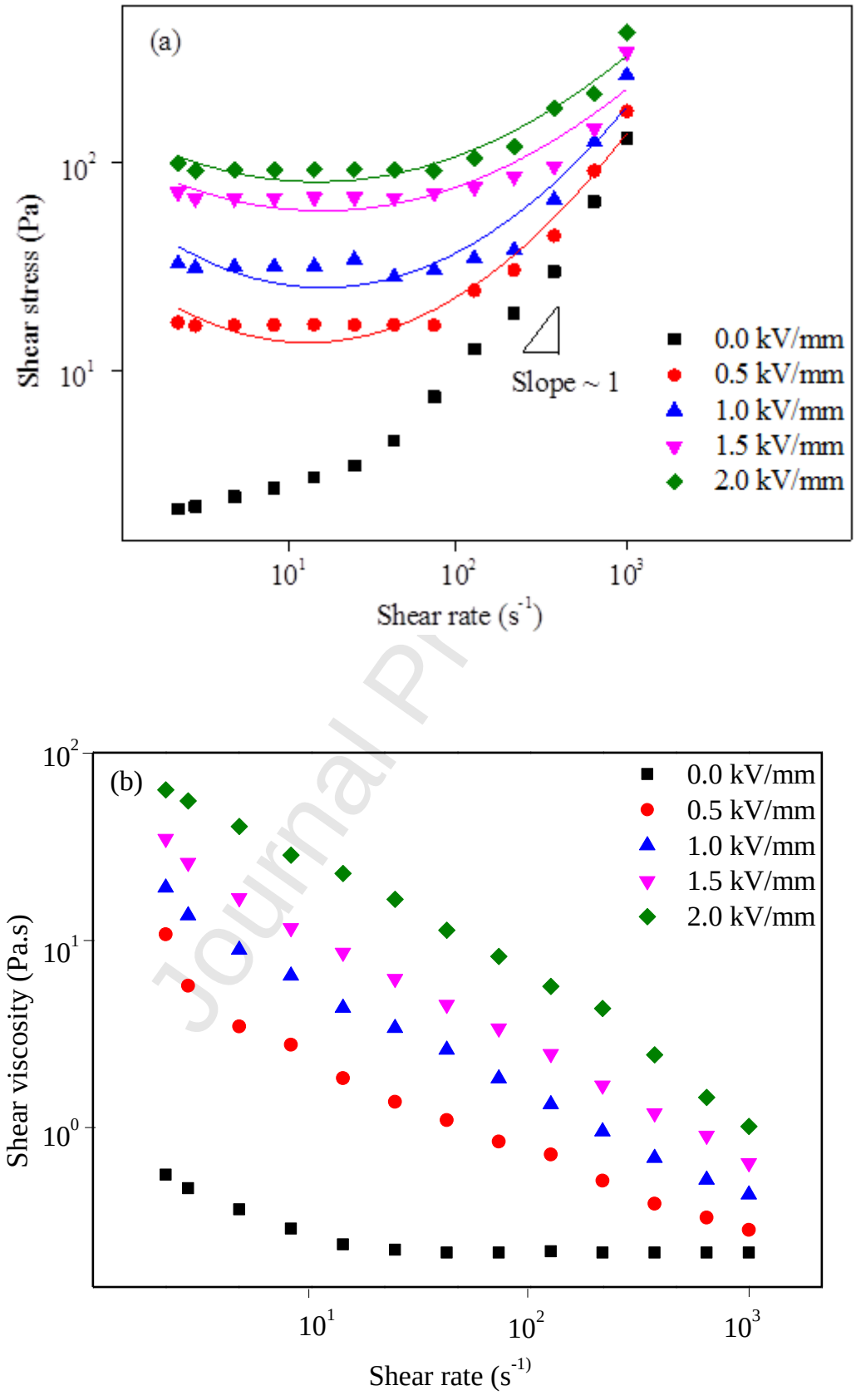

Journal Pre-proof

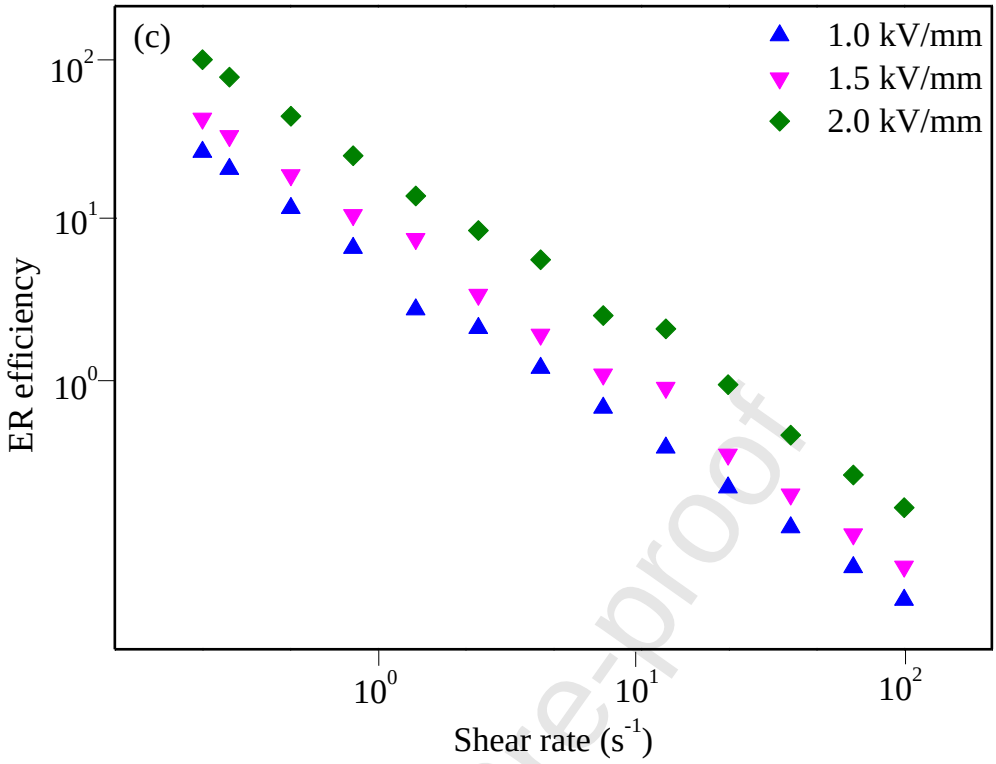

Journal Pre-proof

Figure 10:

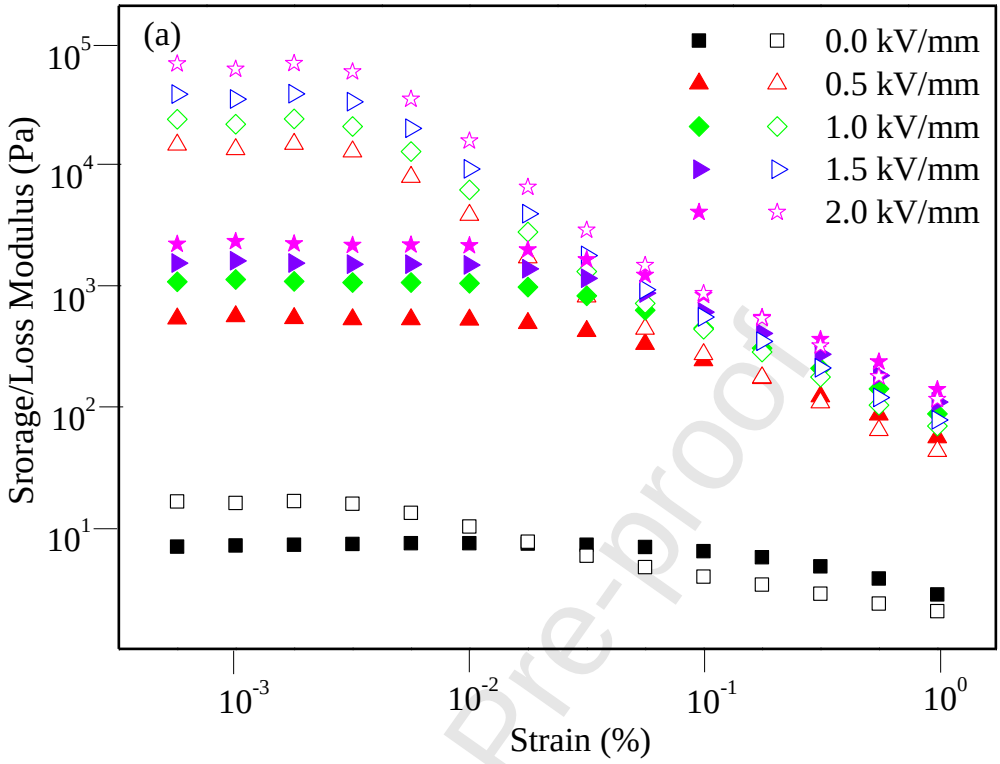

Journal Pre-proof

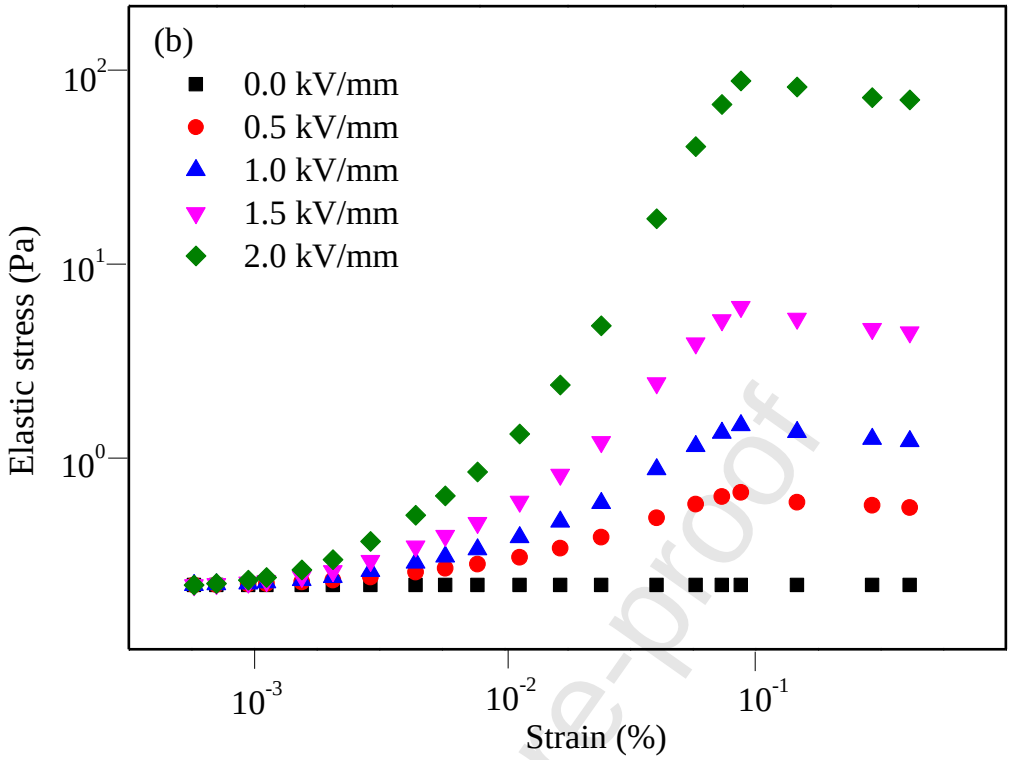

Journal Pre-proof

Figure 11:

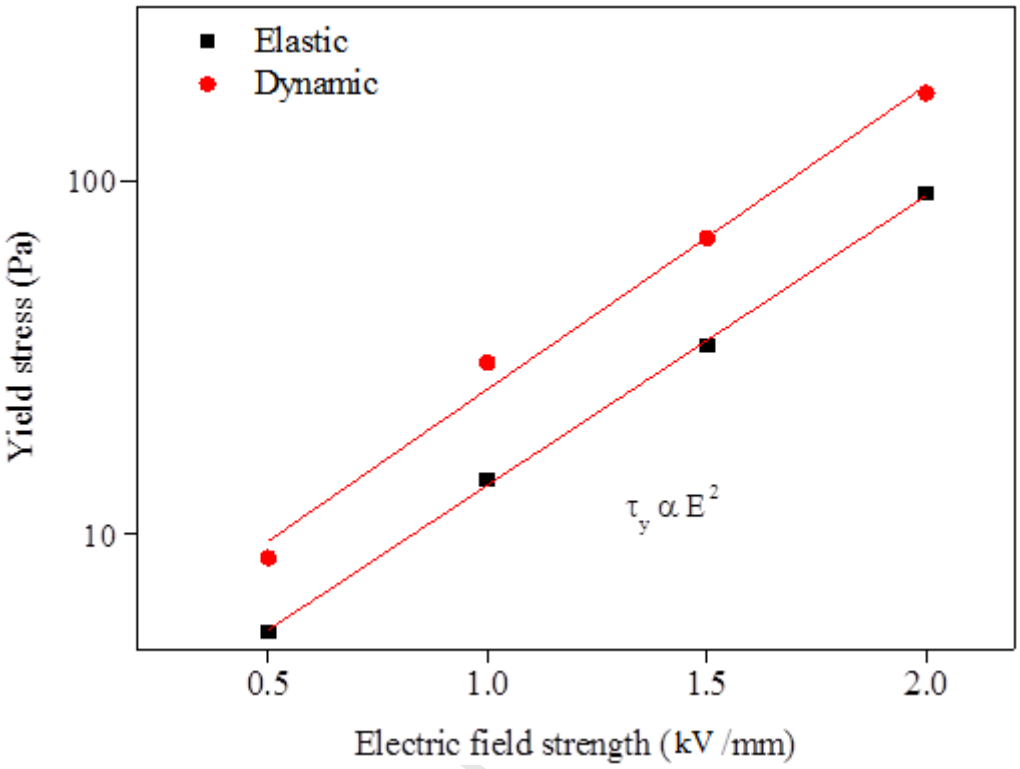

Journal Pre-proof

Figure 12:

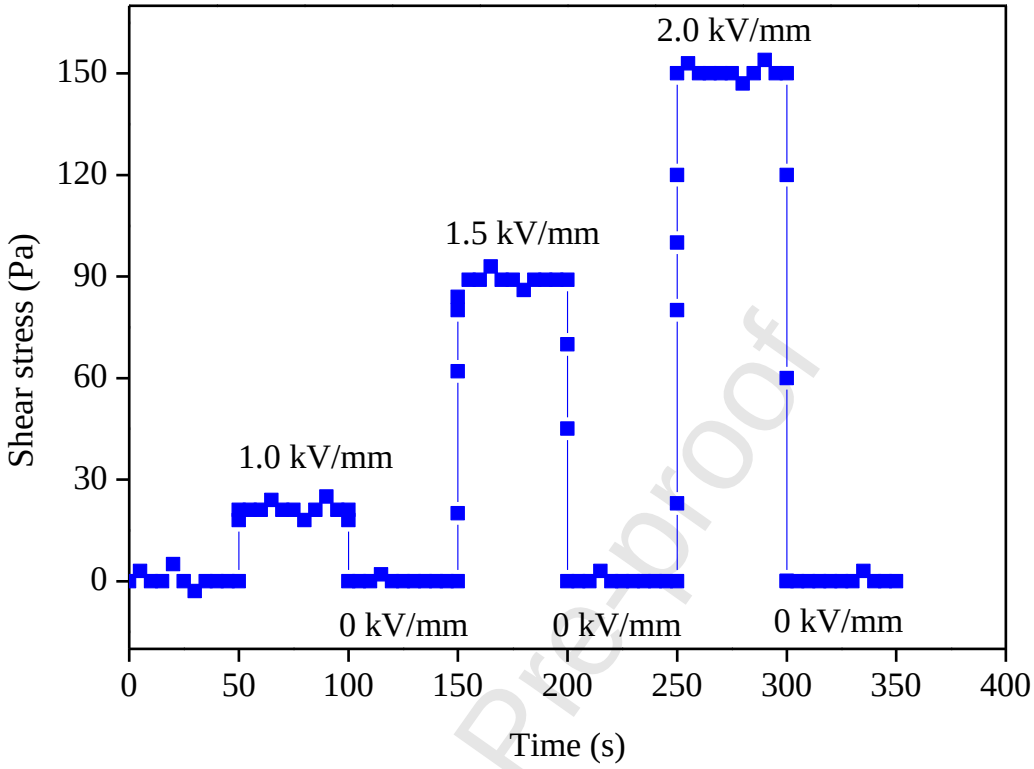

Journal Pre-proof

Figure 13:

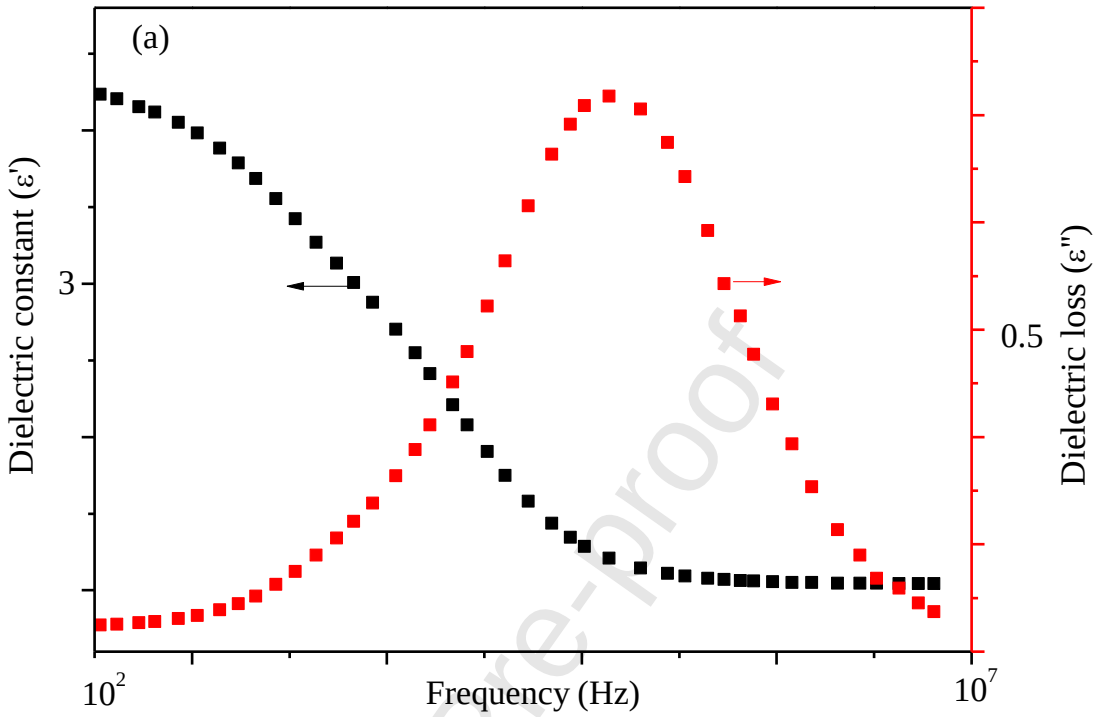

Journal Pre-proof

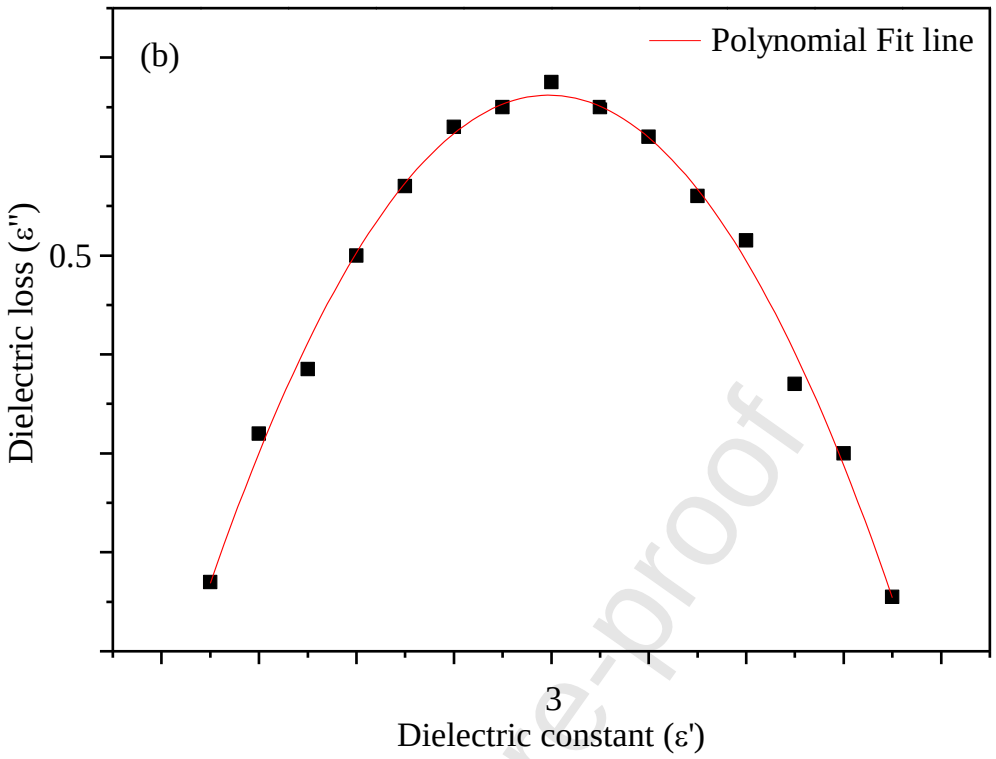

Figure 14:

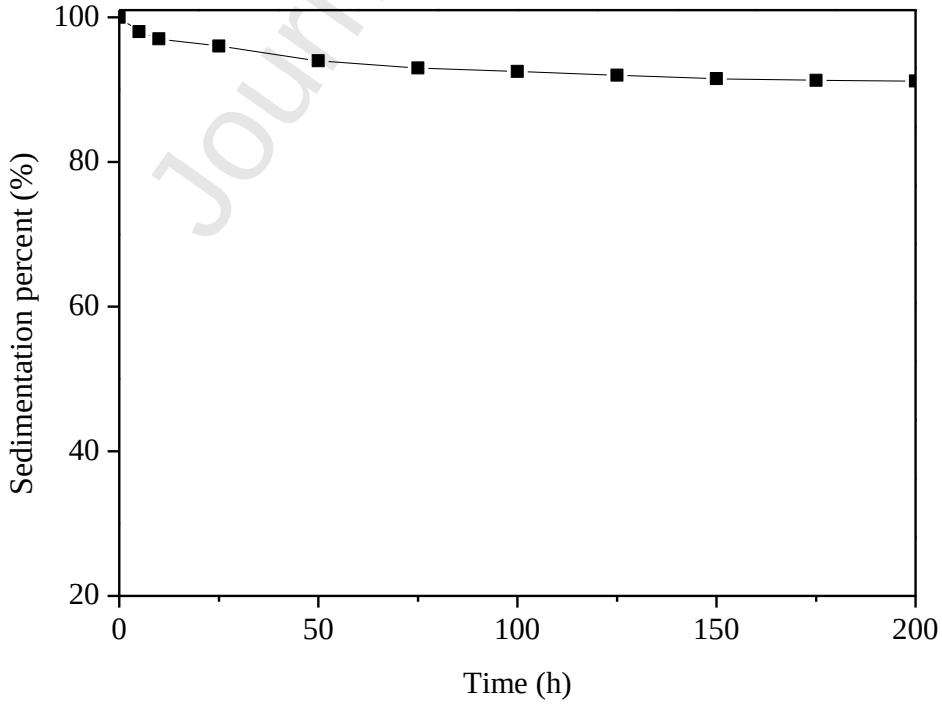

Journal Pre-proof

Table 1

Model	Parameter	Electric field strength (kV/mm)			
		0.5	1	1.5	2
CCJ	τ_0	18.6	35.9	68.3	96.6
	t_1	0.158	0.018	0.013	0.009
	α	0.0046	0.682	0.756	1.819
	η_∞	0.102	0.131	0.19	0.246
	β	0.9868	0.8003	0.726	0.682
	t_2	0.182	0.193	0.226	0.319

Table 2

Parameter	ε_0	ε_∞	$\triangle\varepsilon = \varepsilon_0 - \varepsilon_\infty$	λ	$1-\alpha$
Value	2.56	1.8	0.76	0.00026	0.62

Journal Pre-proof

Author Statement

Cuong Manh Vu: Conceptualization, Methodology, Writing- Original draft preparation; Van-Huy Nguyen: Data curation, Validation. Quang-Vu Bach: Visualization, Investigation, Writing- Reviewing and Editing,

Journal Pre-proof

Conflic of Interest
The authors declare that they have no competing interests.

Journal Pre-proof

Highlights

- Hollow poly (O-toluidine-co-O-phenylenediamine) (POT-Co-OPD) was synthesized via oxidative polymerization reaction.
- Fabricated nanoparticles were applied as a new electrorheological (ER) material.
- Their ER characteristics under various external electric field strengths were examined using a rotational rheometer.
- Their yield stresses was well correlated with universal yield stress equation.

Journal Pre-proof